

- [8] Li, N., and Li, X. R. (2001)
Tracker design based on target perceivability.
IEEE Transactions on Aerospace and Electronic Systems, **37** (2001), 214–225.
- [9] Cong, S., and Hong, L. (1999)
Computational complexity analysis for multiple hypothesis tracking.
Math. Comput. Model., **29** (1999), 1–16.
- [10] Leung, H., Hu, Z., and Blanchette, M. (1996)
Evaluation of multiple target track initiation techniques in real radar tracking environments.
IEE Proceedings—Radar, Sonar Navigation, **143** (1996), 246–254.
- [11] Li, X. R., and Li, N. (2000)
Integrated real-time estimation of clutter density for tracking.
IEEE Transactions on Signal Processing, **48** (2000), 2797–2805.
- [12] Kirubarajan, T., Bar-Shalom, Y., and Pattipati, K. (2001)
Multiassignment for tracking a large number of overlapping objects.
IEEE Transactions on Aerospace and Electronic Systems, **37** (2001), 2–21.

Detection, Location, and Imaging of Fast Moving Targets Using Multifrequency Antenna Array SAR

In this correspondence, we generalize the linear antenna array synthetic aperture radar (SAR) from transmitting single-wavelength signals to transmitting multiple-wavelength signals (called multifrequency antenna array SAR). We show that, using multifrequency antenna array SAR, not only the clutters can be suppressed but also locations of both slow and fast moving targets can be accurately estimated. A robust Chinese remainder theorem (CRT) is developed and used for the location estimation of fast and slowly moving targets. Simulations of SAR imaging of ground moving targets are presented to show the effectiveness of the multifrequency antenna array SAR imaging algorithm.

I. INTRODUCTION

Synthetic aperture radar (SAR) is widely used for imaging of terrain and stationary targets. However,

Manuscript received March 28, 2000; revised August 28, 2001 and July 10 and October 24, 2003; released for publication November 8, 2003.

IEEE Log No. T-AES/40/1/826483.

Refereeing of this contribution was handled by L. M. Kaplan.

The work of C. Wang and X-G. Xia was partially supported by the 1998 Office of Naval Research Young Investigator Program (YIP) Award under Grant N00014-98-1-0644 and ONR N00014-0-110059.

0018-9251/04/\$17.00 © 2004 IEEE

when targets are moving, the motion-induced phase errors cause images of moving targets mis-located in the azimuth dimension and smeared in both the cross-range and the range domains. Several methods, such as space-time-frequency processing [8–9], multichannel SAR [3–6], linear antenna array velocity SAR (VSAR) [1–2], and dual-speed SAR [7] have been proposed to deal with the problem. In multichannel SAR, locations and velocities of moving targets are estimated by using the maximum likelihood (ML) method. For the linear antenna array velocity SAR, the ML method is reduced to the fast Fourier transform (FFT) based detection. However, the location and velocity parameters can only be accurately estimated for slowly moving targets. The joint Stars [16] uses a phased array antenna to detect and locate slow-speed moving targets in the presence of clutter.

In this correspondence, we generalize the linear antenna array SAR from transmitting single-frequency signals into transmitting multifrequency signals, which we call multifrequency antenna array SAR (or MF-SAR for short). MF-SAR forms multiple complex images from different receiving antennas and different wavelengths. Moving targets may be separated in terms of their velocities by using the multiple complex images and, thus, moving targets may be separated from stationary clutter, i.e., clutter can be suppressed. However, the location parameters of moving targets detected using these multiple images from a single frequency SAR may have some ambiguity as appeared in linear antenna array SAR [1–2]. To resolve the ambiguity problem, multiple complex images with multiple frequencies are used and a robust Chinese remainder theorem (CRT) is developed for the phase unwrapping. Furthermore, a condition on the number of the receive antennas, the multiple wavelengths and the maximal velocities of targets is obtained such that the location ambiguities of the moving targets can be resolved. This correspondence is organized as follows. In Section II, the linear antenna array SAR imaging of moving targets and the corresponding problems are addressed. In Section III, MF-SAR and imaging algorithms are introduced. A robust CRT is also developed in this section. It is shown that the locations of moving targets can be accurately estimated with the MF-SAR. In Section IV, we use simulated ground moving targets to demonstrate the theory of MF-SAR.

II. LINEAR ANTENNA ARRAY SAR IMAGING OF MOVING TARGET

In this section, we first briefly review the linear antenna array SAR (or VSAR) for slowly moving targets obtained in [1, 2]. We then discuss the problem associated with estimating the locations of fast moving

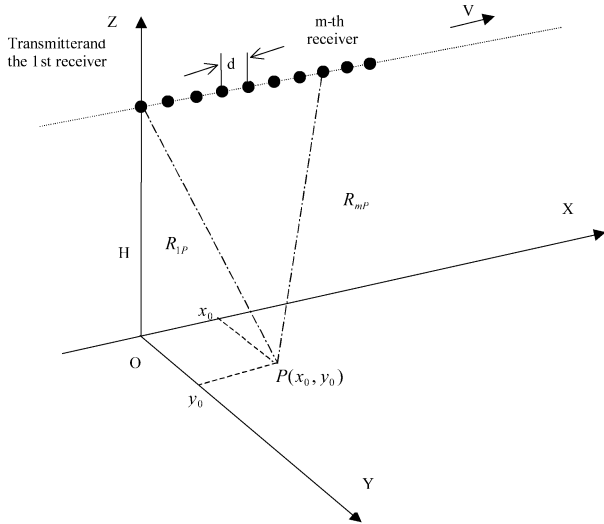


Fig. 1. Geometry of linear antenna array SAR.

targets. Assume that the radar platform flies along a straight line with an altitude H and velocity v . The antennas are located along the direction of the flight track, where M antennas are receiving and one antenna is transmitting. The distance between all the adjacent antennas is assumed d .

We define that the Y axis is along the projection of the radar line of sight on the horizontal plane and the X axis is the azimuth (or cross-range) direction, which coincides with the flight direction of the radar platform as shown in Fig. 1. The radar transmitter is assumed located at $x = 0$ in X direction at time $t = 0$. The instantaneous coordinate (x, y) of the m th receiver at time t is $(x, y) = (vt + (m - 1)d, 0)$.

Suppose that there is a point target P located at point (x_0, y_0) at time $t = 0$, and the target moves with a constant velocity (v_x, v_y) . After the range compression, the removal of some common phase by the knowledge of the antenna distance and the velocity of radar, the complex SAR image of the moving target obtained at the m th receiver from target P can be represented as, see for example [1, 2, 29],

$$S_{m,(x_0,y_0)}(n, l) = \exp \left[-j \frac{4\pi R_0}{\lambda} - j \frac{2\pi}{R_0 \lambda} (m-1)x_0 d \right] \times \delta(n - n_{x_0} - \Delta_{\text{shift}} + (m-1)\Delta_{\text{shift},1}) \times \delta(l - l_{(x_0,y_0)}) \quad (1)$$

where Δ_{shift} is the shift/migration $\Delta = x_0 v_x + y_0 v_y / v$ in the SAR image of the target from the true position n_{x_0} because of the velocity (v_x, v_y) of the target after the quantization by the SAR image resolution ρ_x , i.e., $\Delta_{\text{shift}} = \Delta / \rho_x$, and it is independent of m ; $(m-1)\Delta_{\text{shift},1}$ is the shift/migration of the target in the SAR image at the m th receiver from the SAR image at the first receiver and is a result of the two receiver position difference $(m-1)d$; and $n_{x_0} + \Delta_{\text{shift}} + (m-1)\Delta_{\text{shift},1}$ is the detected position

of the target in the SAR image in the cross-range. Because the shift part $(m-1)\Delta_{\text{shift},1}$ is smaller than one cross-range cell similar to what is explained in [29], it can be neglected. In (1), $l_{(x_0,y_0)}$ stands for the range cell where the target P is located after range compression, $R_0 = \sqrt{h^2 + x_0^2 + y_0^2}$. Compared with the conventional SAR with one receiver, we now have M received signals from M antenna receivers. Using the M received signals, M images are obtained. Multiplying

$$\omega_\lambda(n_{x_0} + \Delta_{\text{shift}}, m) = \exp \left[j \frac{2\pi}{R_0 \lambda} (n_{x_0} + \Delta_{\text{shift}}) \rho_x (m-1)d \right]$$

to (1) and using $x_0 = \rho_x n_{x_0}$, (1) becomes

$$S(m) = S_{m,(x_0,y_0)}(n) = \exp \left[-j \left(\frac{4\pi R_0}{\lambda} - \frac{2\pi \rho_x \Delta_{\text{shift}} (m-1)d}{R_0 \lambda} \right) \right] \times \delta(n - n_{x_0} - \Delta_{\text{shift}}) \quad (2)$$

where m corresponds to the m th antenna receiver. From (2), one can clearly see that the shift Δ_{shift} can be solved by taking the Fourier transform of $S(m)$, $1 \leq m \leq M$, with respect to variable m , under the condition that the shift Δ_{shift} is small enough such that there is no ambiguity due to the 2π modulo operation (folding) in the Fourier transform. The targets with different velocities may be in different image planes, which are called V-images. When Δ_{shift} is solved, the position n_{x_0} of the moving target can be, therefore, solved by subtracting Δ_{shift} from the detected position $n_{x_0} + \Delta_{\text{shift}}$. It can be seen from (2) that, for a stationary target, $\Delta_{\text{shift}} = 0$, i.e., the stationary target is in the 0th velocity image plane in the V-images. There are at least two issues for the accuracy of the solution. The first issue is the maximal range of the solvable Δ_{shift} . If Δ_{shift} is too large, the discrete Fourier transform (DFT) will fold it back due to the 2π modulo operation. One can see that this problem is independent of the number M of the antennas but dependent of the distance d between adjacent antennas. The smaller the distance d is, the larger the detectable range of the shift Δ_{shift} is, i.e., the larger the detectable velocity of a moving target is. On the other hand, the distance also relates to the resolution of the detectable shift Δ_{shift} . The larger the distance is, the better the resolution of the solution of Δ_{shift} is. Moreover, in practice this distance d cannot be too small and thus the maximal detectable shift Δ_{shift} , i.e., the maximal velocity is limited. This is the reason why VSAR in [1, 2] is effective to slowly moving targets, such as walking people, and has problems to fast moving targets, such as vehicles. This issue will be resolved in the next section by using multiple wavelengths λ . The second issue is the resolution of the detected shift Δ_{shift} , i.e.,

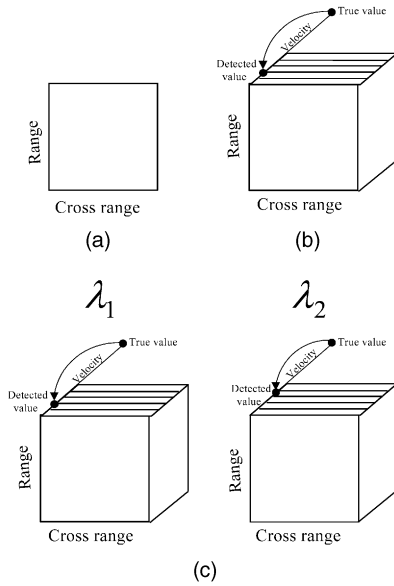


Fig. 2. SAR images of different methods. (a) SAR image. (b) VSAR image. (c) MF-SAR image.

the smallest difference between the distinguishable shifts Δ_{shift} that can be detected through the VSAR. This issue is related to the number M of antennas and the distance d between the adjacent antennas as mentioned previously. The larger the antenna number M is and the larger the distance d is, the better the resolution of the solution of Δ_{shift} is. A detailed relationship was given in [1, 2] and can also be seen later in the work presented here.

III. MULTIFREQUENCY ANTENNA ARRAY SAR

In this section, we present the principle and SAR image algorithm of MF-SAR. The intuitive principle is basically explained in Fig. 2. The conventional SAR image does not contain any velocity information of a moving target as shown in Fig. 2(a) and thus is not able to remove the target image shift/migration in the cross-range. VSAR image contains the velocity information, but it has the ambiguity as shown Fig. 2(b) due to the physical limitation of an antenna array. MF-SAR image can obtain several ambiguous velocities as shown in Fig. 2(c) and the true velocity can be resolved from the multiple ambiguous ones. To analytically explain this, for convenience we first consider MF-SAR imaging of a moving target without clutter. We then discuss the clutter suppression and finally consider MF-SAR of multiple moving targets with clutters.

A. MF-SAR Imaging of Single Moving Target without Clutter

Assume the radar transmits signals with L different carrier wavelengths λ_i for $i = 1, 2, \dots, L$. Then, L series of VSAR images can be obtained. Consider the single

moving target located at (x_0, y_0) with velocity (v_x, v_y) . In this case, (2) becomes

$$S_i(m) = \exp \left[-j \left(\frac{4\pi R_0}{\lambda_i} - \frac{2\pi \rho_{x,i} \Delta_{\text{shift},i} (m-1)d}{R_0 \lambda_i} \right) \right] \quad (3)$$

the detected positions are $n_{x_0} + \Delta_{\text{shift},i}$, $i = 1, 2, \dots, L$, and $\Delta_{\text{shift},i} = \Delta / \rho_{x,i}$, where $\Delta = x_0 v_x + y_0 v_y / v$ independent of an antenna and also independent of a signal wavelength, $\rho_{x,i}$ and $\Delta_{\text{shift},i}$ are the cross-range resolution and the image shift/migration of the moving target with the wavelength λ_i , respectively. For $i = 1, 2, \dots, L$, we define $f_i = \rho_{x,i} \Delta_{\text{shift},i} d / R_0 \lambda_i$. Then, for $i = 1, 2, \dots, L$, from (3) we have

$$S_i(m) = \exp \left(-j \frac{4\pi R_0}{\lambda_i} \right) \exp \left[j \frac{2\pi M f_i (m-1)}{M} \right], \quad m = 1, 2, \dots, M. \quad (4)$$

Equation (4) shows us that the parameter f_i can be estimated by taking M -point DFT of $S_i(m)$.

The M -point DFT of $S_i(m)$ in terms of m gives the residue $\tilde{f}_i = \text{mod}(f_i, 1)$, for $i = 1, 2, \dots, L$. If $f_i < 1$, then $\tilde{f}_i = f_i$, and in this case, there is no ambiguity for the estimated frequency f_i . Otherwise, there is an ambiguity on each estimated frequency from each S_i in (4) due to the modulo operation, i.e., the folding. We next see how the ambiguity can be resolved by using these multiple folded frequencies \tilde{f}_i , $i = 1, 2, \dots, L$.

For each i , instead of the frequency f_i , the estimate of the shift $\Delta_{\text{shift},i}$ of the target is the following residue

$$\text{mod}(\tilde{\Delta}_{\text{shift},i}, M_i) = \text{mod} \left(\frac{\tilde{f}_i R_0 \lambda_i}{\rho_{x,i} d}, M_i \right) = \Delta_{\text{shift},i} \quad (5)$$

where $M_i = R_0 \lambda_i / \rho_{x,i} d$. When all the SAR image resolutions $\rho_{x,i}$ are the same for all different wavelengths λ_i , from the definition of $\Delta_{\text{shift},i}$, we know that all the shifts $\Delta_{\text{shift},i}$ are the same, i.e., $\Delta_{\text{shift},i} = \Delta_{\text{shift}}$ for $i = 1, 2, \dots, L$. In this case, to determine this shift is equivalent to determine its value from its L residues $\text{mod}(\tilde{\Delta}_{\text{shift},i}, M_i) = \Delta_{\text{shift}}$ as in (5) for $i = 1, 2, \dots, L$, which can then be solved by using the CRT. In Section IIID, we discuss how to generate the images with the same resolution in the cross-range from different wavelength λ_i , i.e., $\rho_{x,i} = \rho_x$, $i = 1, \dots, L$, such that, $\Delta_{\text{shift},i} = \Delta_{\text{shift}}$, which is, therefore, always assumed in what follows.

By using the CRT, it is known that the maximal range of the detectable shift Δ_{shift} is

$$\begin{aligned} \max \Delta_{\text{shift}} &= \text{LCM}(M_1, M_2, \dots, M_L) \\ &= \text{LCM} \left(\frac{R_0 \lambda_1}{\rho_x d}, \frac{R_0 \lambda_2}{\rho_x d}, \dots, \frac{R_0 \lambda_L}{\rho_x d} \right) \end{aligned} \quad (6)$$

where LCM stands for the least common multiple. Notice that the above maximal range holds no

matter whether any pair of two different modulus in M_1, M_2, \dots, M_L are coprime or not, see for example [20], while the determination formula in the CRT requires the coprimeness as we see later. Clearly, if all the numbers M_1, M_2, \dots, M_L are coprime each other, then the maximal range of the detectable shift Δ_{shift} is their product $M_1 M_2 \dots M_L$, which reaches the maximum given M_1, M_2, \dots, M_L .

B. Robust Chinese Remainder Theorem

What was studied in the previous subsection gives the basic idea of determining the shift Δ_{shift} from the V-images by using the CRT, which can be stated as follows: when any pair M_i and M_j , $i \neq j$, are coprime and Δ_{shift} satisfies the maximal range (6), it can be formulated as, see for example [23],

$$\Delta_{\text{shift}} = \sum_{i=1}^L \tilde{\Delta}_{\text{shift},i} m_i N_i \quad (7)$$

where $m_i = M_1 \dots M_{i-1} M_{i+1} \dots M_L$, and $\text{mod}(N_i m_i, M_i) = 1$, and $\text{mod}(\tilde{\Delta}_{\text{shift},i}, M_i) = \Delta_{\text{shift}}$ as obtained in (5). The above CRT is based on the assumptions that all M_i are coprime integers and the residues $\tilde{\Delta}_{\text{shift},i}$ are accurate. In practice, these two assumptions may not hold. In particular, when the residues $\tilde{\Delta}_{\text{shift},i}$ are not accurate, the reconstruction in (7) may have large error. Let us see an example. Consider $L = 2$, $M_1 = 3$ and $M_2 = 5$. In this case, $m_1 = 5$ and $N_1 = 2$, $m_2 = 3$ and $N_2 = 2$. Let $\tilde{\Delta}_{\text{shift},1}$ have an error 1 and the other be accurate. The error in Δ_{shift} in (7) is 10. This example tells us that the CRT is not robust. The goal of this subsection is to present a robust CRT for the determination of Δ_{shift} from the L many M -point DFTs in (4), where M_i do not have to be integers, and also present a condition on the number M of antennas and the wavelengths λ_i such that the determination is possible in general.

Based on the discussion in Section IIIA, we always assume that the SAR resolutions in the cross-ranges with different wavelengths are the same, which implies that $\rho_{x,i} = \rho_x$ and $\Delta_{\text{shift},i} = \Delta_{\text{shift}}$. The M -point DFTs in (4) give

$$\tilde{f}_i = \frac{k_i}{M}, \quad \text{for some integer } k_i \text{ with } 0 \leq k_i \leq M-1. \quad (8)$$

Then, the frequencies f_i in (3)–(4) can be written as

$$f_i = n_i + \frac{k_i}{M} + \varepsilon_i \quad (9)$$

where $n_i \geq 0$ are integers and ε_i are the real residual parts and satisfy $|\varepsilon_i| \leq 1/2M$. The migration of a moving target in the VSAR is mainly due to the ambiguous integer part n_i in (9) from the DFT solution. In the following, we want to show how to

resolve this ambiguity using a robust CRT. Let Γ be a positive real number such that

$$\Gamma_i = \Gamma \lambda_i, \quad i = 1, 2, \dots, L \quad (10)$$

are all integers and any pair Γ_i and Γ_j , $i \neq j$, of them are coprime. Note that the above Γ and Γ_i are all known since the wavelengths λ_i are all known. Define

$$F = \frac{\Gamma d \rho_x \Delta_{\text{shift}}}{R_0} \quad (11)$$

where Γ , d , R_0 , ρ_x are all known and F is independent of the wavelength index i . Thus, to determine Δ_{shift} we only need to determine F . From (9), F can be written as

$$F = n_i \Gamma_i + \frac{k_i \Gamma_i}{M} + \varepsilon_i \Gamma_i, \quad i = 1, 2, \dots, L. \quad (12)$$

Clearly, to determine F we need to determine n_i and ε_i . One can see that an incorrect n_i induces a large scale migration of the scatterer while an incorrect ε_i only induces a small scale precision of the scatterer. In the following, we present a robust CRT to determine n_i and a condition on the number M of antennas and the wavelengths such that n_i can be uniquely determined. On the other hand, the small scale error ε_i part cannot be determined from the DFTs and therefore it is ignored but we present an error estimate of the shift Δ_{shift} due to this ignorance. In what follows, an error on the integer part n_i is called a large scale migration and an error on the fractional residual part ε_i is called a small scale precision error.

For $i = 1, 2, \dots, L$, let

$$\gamma_i = \Gamma_1 \dots \Gamma_{i-1} \Gamma_{i+1} \dots \Gamma_L. \quad (13)$$

Without loss of generality, we assume

$$\Gamma_1 < \Gamma_2 < \dots < \Gamma_L. \quad (14)$$

For $i = 2, 3, \dots, L$, let S_i be the set of pair integers (\bar{n}_1, \bar{n}_i) in the range $0 \leq \bar{n}_1 \leq \gamma_1 - 1$ and $0 \leq \bar{n}_i \leq \gamma_i - 1$ such that

$$\begin{aligned} & \left| \bar{n}_i \Gamma_i + \frac{k_i \Gamma_i}{M} - \bar{n}_1 \Gamma_1 - \frac{k_1 \Gamma_1}{M} \right| \\ &= \min_{\substack{0 \leq \hat{n}_1 \leq \gamma_1 - 1 \\ 0 \leq \hat{n}_i \leq \gamma_i - 1}} \left| \hat{n}_i \Gamma_i + \frac{k_i \Gamma_i}{M} - \hat{n}_1 \Gamma_1 - \frac{k_1 \Gamma_1}{M} \right| \end{aligned} \quad (15)$$

i.e.,

$$S_i =$$

$$\left\{ (\bar{n}_1, \bar{n}_i) = \arg \min_{\substack{0 \leq \hat{n}_1 \leq \gamma_1 - 1 \\ 0 \leq \hat{n}_i \leq \gamma_i - 1}} \left| \hat{n}_i \Gamma_i + \frac{k_i \Gamma_i}{M} - \hat{n}_1 \Gamma_1 - \frac{k_1 \Gamma_1}{M} \right| \right\}. \quad (16)$$

Defining the sets S_i is basically searching the optimal pairs (\bar{n}_1, \bar{n}_i) in the sense of (16) in the finite range $0 \leq \bar{n}_1 \leq \gamma_1 - 1$ and $0 \leq \bar{n}_i \leq \gamma_i - 1$. We now want

to connect this finite range with the maximal range of Δ_{shift} , which is intuitively given in (6). From (10)–(13), it is not hard to see that the following maximal range condition (17) on Δ_{shift} ensures that the true solution of n_i in (12) falls in the range $0 \leq \bar{n}_1 \leq \gamma_1 - 1$ and $0 \leq \bar{n}_i \leq \gamma_i - 1$, i.e., the true solution falls in the sets S_i :

$$\Delta_{\text{shift}} \leq \frac{R_0}{d\rho_x \Gamma} \Gamma_1 \Gamma_2 \cdots \Gamma_L. \quad (17)$$

Let $S_{i,1}$ be the set of all the first components \bar{n}_1 of the pairs (\bar{n}_1, \bar{n}_i) in S_i and S be the intersection of all $S_{i,1}$, i.e., $S = \bigcap_{i=2}^L S_{i,1}$. Then, the following theorem is a robust CRT that determines the solutions n_i and therefore the shift Δ_{shift} .

THEOREM 1 *If the shift Δ_{shift} is in the range (17) and the number M of the receiving antennas satisfies condition*

$$M > \max\{\Gamma_1, \dots, \Gamma_L\} + \min\{\Gamma_1, \dots, \Gamma_L\} \quad (18)$$

then, the set S contains only the element n_1 , i.e., $S = \{n_1\}$, and each set S_i has and only has one pair (\bar{n}_1, \bar{n}_i) with $\bar{n}_1 = n_1$, and furthermore the second element \bar{n}_i in the pair (n_1, \bar{n}_i) is $\bar{n}_i = n_i$, where n_i , $i = 1, 2, \dots, L$, are the solutions in (12). In this case, the solution of Δ_{shift} is given by

$$\tilde{\Delta}_{\text{shift}} = \frac{R_0}{d\rho_x} \frac{1}{L} \sum_{i=1}^L \left(n_i \lambda_i + \frac{k_i \lambda_i}{M} \right) \quad (19)$$

where k_i are solved from the M -point DFTs in (4) and (8).

A proof of this theorem is in the Appendix. This theorem tells us that when the number of antennas and the wavelengths satisfy (18) and the shift Δ_{shift} is in the range in (17), the moving target migration ambiguity can be resolved to a certain precision due to the ignorance of ε_i in (12), i.e., there is not any large scale migration but there may be small scale precision error as shown below. Using (10) and (12), the accuracy of the solution in (19), i.e., the small scale precision error, can be estimated as

$$|\tilde{\Delta}_{\text{shift}} - \Delta_{\text{shift}}| \leq \frac{R_0}{2Md\rho_x} \frac{1}{L} \sum_{i=1}^L \lambda_i. \quad (20)$$

Theorem 1 also tells us an algorithm to determine the integers n_i in (12) and therefore Δ_{shift} as follows.

A Robust Chinese Remainder Theorem Algorithm

Step 1 Input integers k_i in (8) obtained from the M -point DFTs in (4).

Step 2 From the wavelengths λ_i , $i = 1, 2, \dots, L$, determine the number Γ and the integers Γ_i , $i = 1, 2, \dots, L$, in (10), sorted with the order in (14).

Step 3 Determine the sets S_i , $i = 2, 3, \dots, L$.

Step 4 Determine the sets $S_{i,1}$, $i = 2, 3, \dots, L$, and the set S above theorem 1. The element in S is n_1 .

Step 5 For each i , $2 \leq i \leq L$, find the pair (n_1, \bar{n}_i) in S_i and $n_i = \bar{n}_i$.

Step 6 Determine Δ_{shift} using the formula in (19).

Although the complexity of the above robust CRT is higher than the CRT, it is robust and does not require that M_i in (5) are integers as explained before. We now go back to the maximal range (17) of the shift Δ_{shift} , which is basically the same as the one in (6). In terms of the maximal detectable target velocity, from the definition of Δ_{shift} , we have $\Delta_{\text{shift}} = x_0 v_x + y_0 v_y / \rho_x v$. In general, x_0 and the X-direction velocity v_x of the target are negligible, respectively, compared with the distance y_0 and the radar platform velocity v , where y_0 is approximately $y_0 \approx R_0$, the distance between the radar and the target. Thus, $\Delta_{\text{shift}} \approx R_0 v_y / \rho_x v$.

With this approximation, L wavelengths λ_i , and the maximal detectable shift range (17), the maximal detectable velocity v_y in the range direction is

$$\max |v_y| = \frac{1}{2} \frac{v}{d\Gamma} \Gamma_1 \Gamma_2 \cdots \Gamma_L \quad (21)$$

where the factor 1/2 is because there are two different possible directions of v_y .

As a remark, condition (18) on the number of receiving antennas is a sufficient condition for a moving target and it may not be necessary for some moving targets as we shall see in the simulation examples in Section IV. It should be emphasized that the number M of the receiving antennas does not affect the large scale migration resolution as long as it satisfies condition (18), and it, however, affects the small scale precision as we can see from the error estimate.

C. Clutter Rejection

In moving target SAR imaging, clutter rejection is an important step, in particular when the signal to clutter ratio is not too high. Clutters are usually suppressed before the moving target detection and imaging. Since clutters are stationary, as we discussed in Section II all clutters are imaged in the 0th velocity image in all V-images while we will see in Section III E that a moving target cannot be removed in all the V-images. Therefore, they can be suppressed by removing the 0th velocity image plane in V-images. We see simulation results in Section IV.

D. Uniform Cross-Range Resolution with Transmitted Signals of Different Carrier Wavelengths

The SAR image resolution ρ_x depends on the wavelength and the aperture size in, for example, the spotlight SAR as we see later. Therefore, even when all the antenna aperture sizes are the same, V-images may have different resolutions $\rho_{x,i}$ for different wavelengths λ_i . As we explained in Section III A, it

is important to unify the resolutions of V-images in the cross-range such that they are independent of a wavelength. We next want to see stripmap SAR and spotlight SAR.

In the stripmap SAR, the resolution ρ_a in the cross-range direction is $D/2$ that is determined by the radar real aperture D , which is independent of the pulse frequency.

In the spotlight SAR, the resolution in the cross-range is $\rho_a = 0.89\lambda/4\sin(\Delta\theta/2)$, which increases proportionally to the wavelength λ and decreases proportionally to $\sin(\Delta\theta/2)$, where $\Delta\theta$ is the view angle. In order to have the same cross-range resolution of the image with different wavelengths, the view angle (aperture length) should be different accordingly, which can be achieved by adjusting the time duration length in SAR imaging. As a remark, in both stripmap SAR and spotlight SAR, the interpolation is needed for coherent multiple V-images in practice.

E. Multiple Moving Target Image Registration

In the previous subsections, we discussed MF-SAR imaging of a single moving target. In general, there may be multiple moving targets. As we have seen in Section IIIA, if all the V-images only include a single target, the CRT can be used to estimate the correct position of the target. This implies that, if all the multiple targets can be coherently separated in V-images so that different individual moving targets are included in different sets of V-images and then each moving target location can be estimated using the MF-SAR for a single moving target as in Section IIIA. The target separation procedure is called multiple moving target image registration. We next explain how the image registration is done by considering two moving targets and two sets V-images obtained from two different wavelengths λ_1 and λ_2 , which is basically illustrated in Fig. 3.

1) *None of Moving Targets is Imaged in the 0th Velocity Image Plane:* We first consider the case when none of the moving targets is imaged in the 0th velocity image plane in V-images. In this case, there are three subcases as shown in Fig. 3, which are discussed as follows.

Case 1 Different moving targets are imaged in different range cells as shown in Fig. 3(a). In this case, it is not hard to see from the SAR imaging that the targets can be separated in V-images according to the range cells because the images of a target P must have the same range cell number in the V_1 -image with wavelength λ_1 and V_2 -image with wavelength λ_2 . Therefore, the registration of V_1 -image and V_2 -image of two targets can be obtained via range cell by range cell imaging.

Case 2 Different moving targets are imaged in different cross-range cells as shown in Fig. 3(b). This case is similar to Case 1.

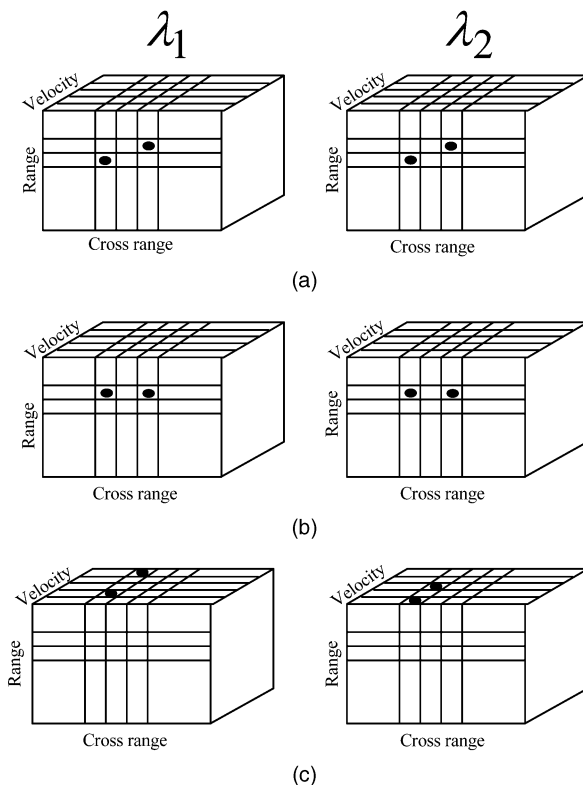


Fig. 3. Multiple moving target image registration. (a). (b). (c).

Case 3 Different moving targets are imaged in the same range cell and the same cross-range cell as shown in Fig. 3(c).

Although it is impossible to have two moving targets at the same position, i.e., the same range and the cross-range, it may be possible to have two moving targets located at the same range bin but different locations x_1 and x_2 in the cross-range and with different velocities. The different velocities may induce the different shifts Δ_{shift_1} and Δ_{shift_2} , which may cause the two targets imaged at the same range and the same cross range cell as shown in Fig. 3(c). There are two subcases here.

Case 3(a) The reflectivity of the two targets is significantly different. In this case, the image registration can be done according to the different magnitudes of the images of different targets.

Case 3(b) The reflectivity of two moving targets is not significantly different. In this case, the image registration cannot be done, i.e., the multiple moving targets cannot be separated, before implementing the CRT for each individual target as in Cases 1–2. In this case, the CRT for a single number determination from its multiple residues should be generalized to multiple number determination from their multiple residue sets, which has been recently obtained in [20–22]. Since the probability of Case 3(b) is small in practice, we do not describe the generalized CRT for multiple targets here. We, however, refer the reader to [20–22]. As a result, this approach might be used to isolate moving

scatters that may possibly overlap in both range and cross-range cells.

2) *Some Moving Targets are Imaged in the 0th Velocity Image Plane:* Since the clutter rejection is achieved by removing the 0th velocity image in V-images, if some targets are imaged in the 0th velocity images, they are also removed during the clutter rejection. We next want to show that a moving target cannot be removed in all the L V-images during the clutter rejection under the maximal velocity constraint (21), unless its image does not have a shift from its true position.

For each target, there are L V-images with different velocity bins, where L is the wavelength number. Assume the maximal velocity of all moving targets satisfies condition (21), or in other words, the maximal image shift of the moving targets satisfies (6). If there exists a moving target such that it is in the 0th velocity image in all V-images, i.e., $\Delta_{\text{shift},i} = 0 = \Delta_{\text{shift}} \bmod M_i$, $i = 1, 2, \dots, L$, in other words $\Delta_{\text{shift}} = k_i M_i$, $i = 1, 2, \dots, L$. Therefore, we have $\Delta_{\text{shift}} = k \text{LCM}(M_1, M_2, \dots, M_L)$. By (6), we conclude that $k = 0$, i.e., $\Delta_{\text{shift}} = 0$, which means that the target does not have a shift/migration/move in its SAR image, i.e., it is correctly positioned. On the other hand, it also proves that for a moving target in the SAR image, there must exist L_1 with $0 < L_1 \leq L$ such that $\Delta_{\text{shift},i_k} \neq 0 \pmod{M_{i_k}}$ for $k = 1, 2, \dots, L_1$, which implies that a moving target will not be in all the 0th velocity V-images, i.e., it is not removed during the clutter rejection. The method we used to determine whether a moving target is removed in a 0th velocity V-image is to compare the magnitudes of the target in all the 0th velocity V-images. The above analysis also implies the importance of using more than one wavelength in the antenna array SAR. Otherwise, moving targets may be removed in the clutter rejection.

F. MF-SAR Algorithm

We now present an algorithm for MF-SAR imaging of moving targets. For simplicity, we only consider the case of two wavelengths, which can be easily generalized to the L wavelength case. The block diagram is shown in Fig. 4.

Step 1 Radar transmits linear frequency modulated (LFM) (or step frequency) signals with carrier wavelengths λ_1 and λ_2 alternatively. M return signals from M receiving antennas are received.

Step 2 The range compression is implemented to the M received signals. And phase $\xi_{1,\lambda}(t)$ is compensated, where

$$\xi_{1,\lambda}(t) = \exp \left\{ j \frac{2\pi}{R_0 \lambda} [v^2 t^2 + 0.5 d^2 (m-1)^2 + vt(m-1)d] \right\}.$$

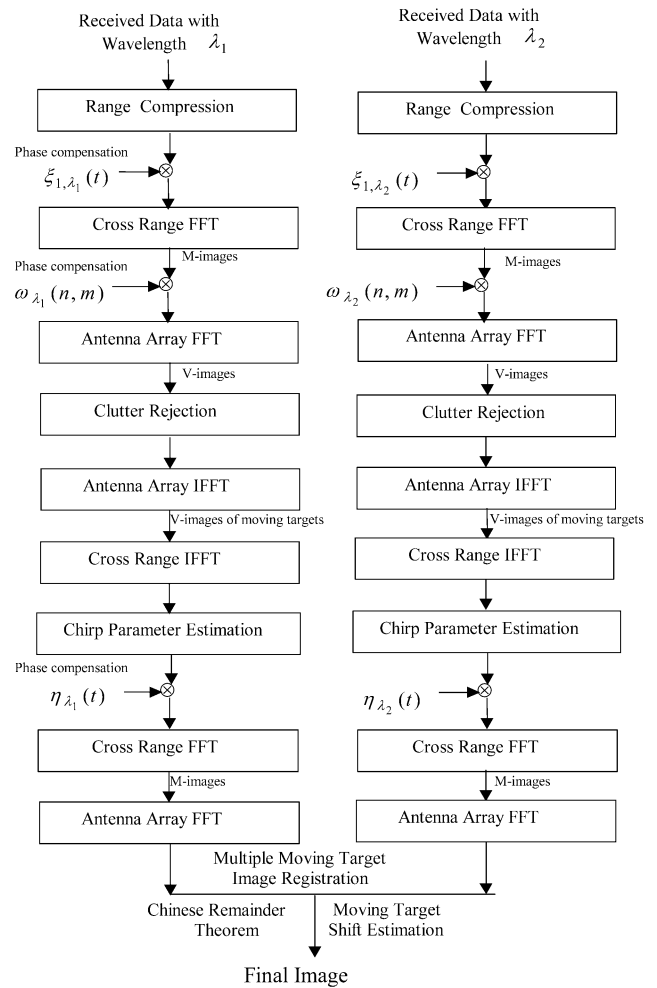


Fig. 4. MF-SAR imaging algorithm.

Step 3 The Fourier transform in the cross-range direction is taken to obtain M conventional SAR images, i.e., M -images, for each wavelength λ_i .

Step 4 The image phase $\omega_{\lambda}(n, m)$ before (2) is compensated in the M -images to remove the image frequency of the stationary targets in the antenna array direction.

Step 5 The Fourier transform in the antenna array direction is taken to get the V-images. The stationary targets are imaged in the 0th velocity image plane in all the V-images.

Step 6 Clutter rejection is implemented by removing the zero velocity image plane in V-images.

Step 7 The clutter rejected V-images are transformed back to the range-time domain by taking the inverse Fourier transform in the antenna array direction and then the inverse Fourier transform in the cross-range direction.

Step 8 Chirp rates of signals are estimated and the corresponding phase $\eta_{\lambda}(t)$ is removed.

Step 9 The Fourier transforms in the cross-range and the antenna array direction are taken to obtain new V-images.

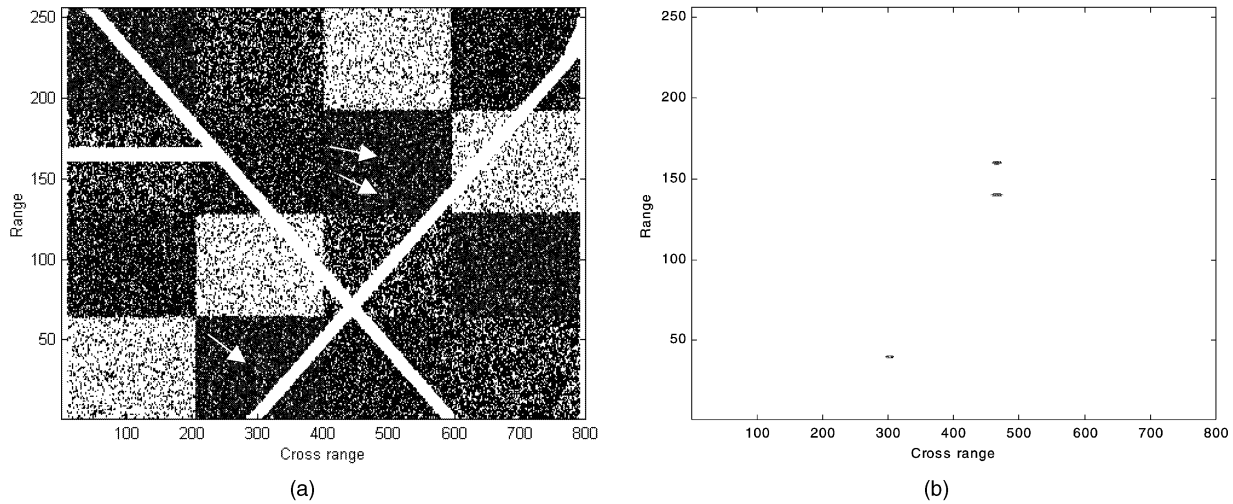


Fig. 5. Conventional SAR image results. (a) Image of targets and ground. (b) Image of target.

Step 10 Implement the multiple target image registration of the new V-images and resolve the velocity ambiguity by using the robust CRT algorithm in Section IIIB.

Step 11 Remove the image shift in the cross range direction to get the correct image.

IV. SIMULATION RESULTS

In this section, we want to present simulation of the MF-SAR imaging proposed here. The parameters used in the simulation are: radar speed $v = 200$, radar height $H = 4000$ m, wavelengths $\lambda_1 = 0.03$ m, $\lambda_2 = 0.05$ m, pulse repetition frequency $f_{\text{prf}} = 800$ Hz, radar bandwidth $B = 40$ MHz, so the range resolution is about 4 m, distance of the adjacent receivers $d = 2$ m, distance of radar targets $R_0 \approx 10000$ m. In this case, the maximal velocity in the range direction in (21) is 7.5 m/s. The sufficient condition (18) on the number of antennas is $M > 3 + 5 = 8$.

In the simulation, there are three moving targets on the roads with speed 3 m/s, 7 m/s, and 10.5 m/s, respectively. The first road is parallel to the radar flying direction. The second and the third road have the 45° and 135° angle with the radar flying direction, respectively. The first and the second targets move away from the radar on the second road. The third target moves towards to the radar on the third road. The corresponding velocities v_y in the range direction are 2.1 m/s, 5 m/s, and -7.4 m/s, which are all in the maximal range. The reflectivity of the moving targets is 2 times of the reflectivity of the ground clutters. Total $M = 5$ antennas are used, which is below the one 9 in the sufficient condition (18), which means that some moving targets can be well imaged even the number of antenna is less than the sufficient condition, i.e., this condition is not necessary. Let

the synthetic aperture length be T_i corresponding to the wavelength λ_i with $T_1 \lambda_2 = T_2 \lambda_1$, so that the cross resolutions with different carrier frequency are the same.

Fig. 5(a) shows the moving target and ground imaging results of the conventional SAR with wavelength λ_1 , where one can see the shifts in the cross-range of the moving targets and all three moving targets are imaged out of the roads. It is hard even to find the moving targets. Fig. 5(b) shows the conventional SAR imaging of the moving targets without the clutter. Fig. 6(a) shows the moving target and ground imaging results of the VSAR with wavelength λ_2 . The maximal velocity in the range direction so that there is no migration of the moving target in the VSAR image is 2.5 m/s. One can see that the range direction velocity of the first target is below this maximal one while the two range velocities of the other two targets are above this maximal one. Fig. 6(b) shows the VSAR imaging results of the moving targets without clutter, where from Fig. 6(a)–(b) one can see that the first one is correctly located while the other two are mis-located off the roads.

To illustrate the clutter suppression of MF-SAR, Fig. 7(a) shows the imaging results of the clutters after the clutter and the targets separation in Fig. 3, and Fig. 7(b) shows the moving target imaging resulted from using MF-SAR after the clutter and the target separation in the V-image domain. Fig. 7(a) and Fig. 7(b) tell us that the clutter and the moving targets can be well separated. This also means the clutter and the moving target separation improves the signal to clutter ratio in the signal after the clutter rejection. Fig. 7(c) shows the final imaging results of the three ground moving targets by using the MF-SAR algorithm, where the three moving targets are accurately located on the roads.

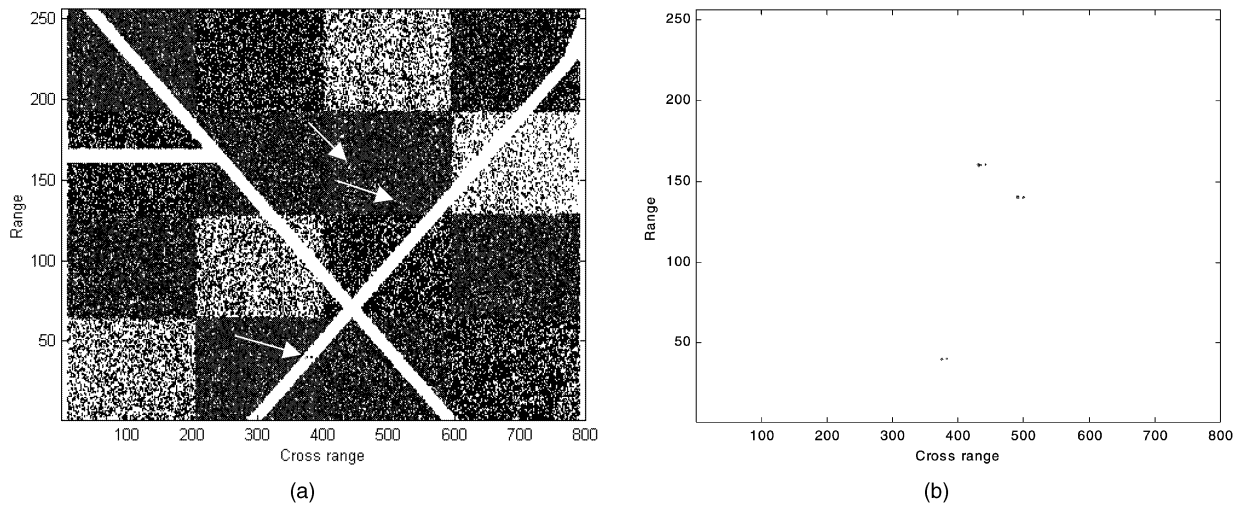


Fig. 6. VSAR imaging results. (a) Image of targets and ground. (b) Image of targets.

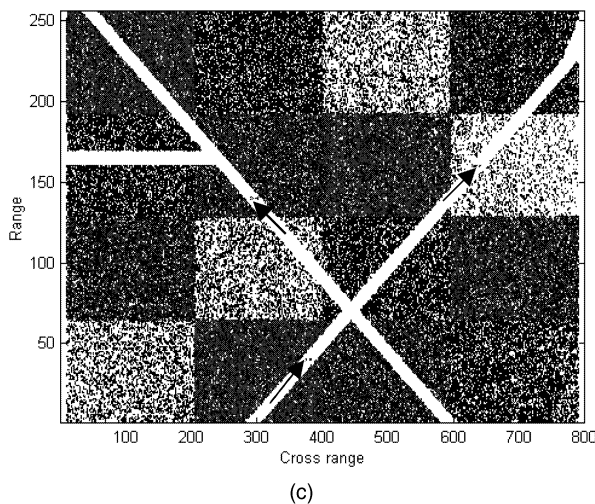
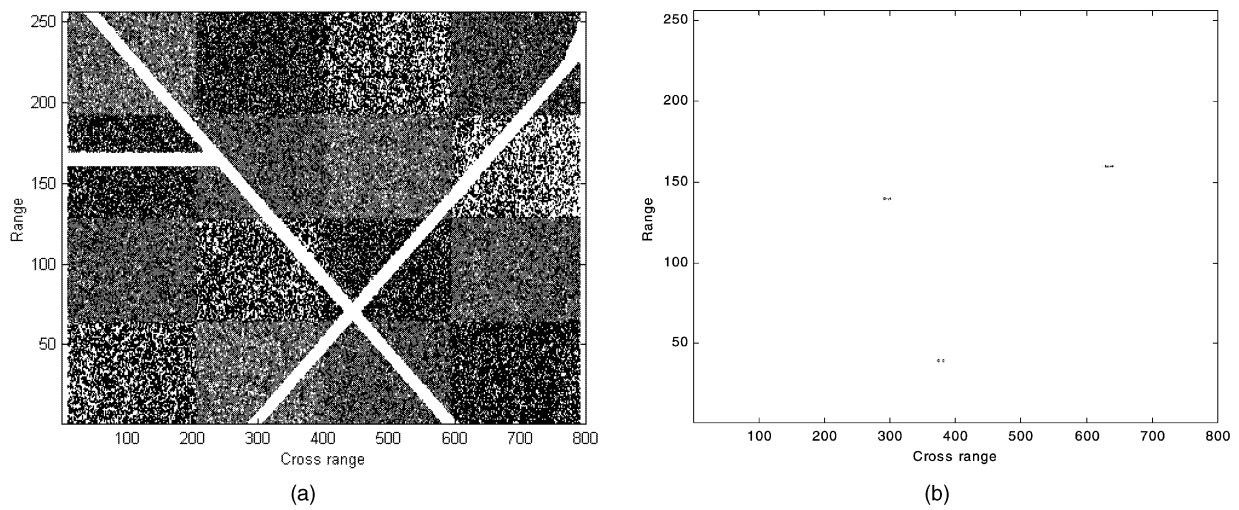


Fig. 7. MF-SAR imaging results. (a) Image of ground. (b) Image of targets. (c) Image of targets and ground.

V. CONCLUSIONS

In this correspondence, we have proposed an MF-SAR imaging method of moving targets. In the MF-SAR, the radar transmits signals with multiple wavelengths, which is a generalization of the existing

multichannel SAR and VSAR obtained in [1–6]. A robust CRT has been developed for removing the ambiguities of the moving targets. Furthermore, a condition on the number of receiving antennas and multiple wavelengths and the maximal range of moving velocities of targets have been obtained such

that the location ambiguities of the moving targets can be resolved. We have shown that the MF-SAR is able to accurately locate and image both ground moving targets with fast and slow velocities with a reasonable number of receiving antennas. In our simulation, five receiving antennas were used in the ground moving target imaging and the targets move in constant velocities. In this paper, we have also studied the clutter and target separation, i.e., clutter rejection. Both theoretical and simulation results have shown that the MF-SAR is a promising technique for fast ground moving. However, more tests are certainly needed to evaluate this approach in practice on real data where 1) the targets may not have constant velocities and 2) the clutter may not be easily removed by removing the 0th velocity image as what was done in this approach. Also, when the number of receive antennas is large, there may be difficulties in the implementation.

APPENDIX (PROOF OF THEOREM 1)

When (17) holds for Δ_{shift} , from (11)–(13) it is not hard to see that $0 \leq n_i < \gamma_i$, $i = 1, 2, \dots, L$, where n_i are from (12). Therefore, for $i = 2, 3, \dots, L$, and $(\bar{n}_1, \bar{n}_i) \in S_i$ we have

$$\left| \bar{n}_i \Gamma_i + \frac{k_i \Gamma_i}{M} - \bar{n}_1 \Gamma_1 - \frac{k_1 \Gamma_1}{M} \right| \leq \left| n_i \Gamma_i + \frac{k_i \Gamma_i}{M} - n_1 \Gamma_1 - \frac{k_1 \Gamma_1}{M} \right|. \quad (22)$$

Let $\mu_{n_i} = \bar{n}_i - n_i$, $i = 1, 2, \dots, L$. Then, from (10), (12), and (22) we have

$$|\mu_{n_i} \Gamma_i - \mu_{n_1} \Gamma_1| \leq 2|\varepsilon_i \Gamma_i - \varepsilon_1 \Gamma_1| \leq \frac{\Gamma_i + \Gamma_1}{M} < 1, \quad i = 2, 3, \dots, L. \quad (23)$$

Notice that Γ_i and Γ_1 are coprime for $i = 2, 3, \dots, L$ and μ_{n_i} , $i = 1, 2, \dots, L$, are all integers. Equation (23) implies

$$\mu_{n_i} \Gamma_i = \mu_{n_1} \Gamma_1, \quad i = 2, 3, \dots, L. \quad (24)$$

Since Γ_i and Γ_1 are coprime, (24) implies

$$\begin{aligned} \mu_{n_i} &= k \Gamma_i & \text{and} & & \mu_{n_1} &= k \Gamma_1 \\ \text{for } k &= 0, \pm 1, \dots, \pm \min\{\gamma_i, \gamma_1\} - 1. \end{aligned}$$

This implies that

$$S_i = \{(n_1 + k \Gamma_i, n_i + k \Gamma_1) : k = 0, \pm 1, \dots, \pm \min\{\gamma_i, \gamma_1\} - 1\}. \quad (25)$$

From (25), we find that

$$\begin{aligned} \bar{n}_i - n_1 &= k \Gamma_i, & i &= 2, 3, \dots, L \\ \text{and } k &= 0, \pm 1, \dots, \pm \min\{\gamma_i, \gamma_1\} - 1. \end{aligned}$$

In other words, $\bar{n}_i - n_1$ divides all Γ_i , $i = 2, 3, \dots, L$, and therefore from (13), we conclude that $\bar{n}_i - n_1$

is a multiple of γ_1 . Since $0 \leq \bar{n}_1$, $n_1 \leq \gamma_1 - 1$, it is only possible if $\bar{n}_i - n_1 = 0$, i.e., $\bar{n}_i = n_i$. This proves that when (17) and (18) hold, $S = \{n_1\}$. On the other hand, $\bar{n}_1 = n_1$ implies that $k = 0$ in (25), i.e., $\bar{n}_i = n_i$, $i = 2, 3, \dots, L$. This proves Theorem 1.

GENYUAN WANG
XIANG-GEN XIA
 Dept. of Electrical and Computer Engineering
 University of Delaware
 Newark, DE 19716
 E-mail: (giuang,xia@ee.udel.edu)
VICTOR C. CHEN
RALPH L. FIEDLER
 Naval Research Laboratory
 Washington, DC 20375

REFERENCES

- [1] Friedlander, B., and Porat, B. (1997) VSAR: A high resolution radar system for detection of moving targets. *IEE Proceedings—Radar, Sonar Navigation*, **144**, 4 (1997), 205–218.
- [2] Friedlander, B., and Porat, B. (1998) VSAR: A high resolution radar system for ocean imaging. *IEEE Transactions on Aerospace and Electronic Systems*, **34**, 3 (1998), 755–776.
- [3] Ender, J. (1993) Detectability of slowly moving targets using a multi-channel SAR with an along-track antenna array. In *Proceedings of SEE/IEE Conference (SAR 93)*, Paris, May 1993, 19–22.
- [4] Ender, J. (1996) Detection and estimation of moving target signals by multi-channel SAR. *EUSAR'96 Conference*, Konigswinter, 1996, 411–417.
- [5] Rieck, W. (1996) SAR imaging of moving targets: application of time-frequency distribution for single- and multi-channel data. *EUSAR'96 Conference*, Konigswinter, 1996, 431–434.
- [6] Lombardo, P. (1997) Estimation of target motion parameters from dual-channel SAR echoes via time-frequency analysis. In *Proceedings of the National Radar Conference*, 1997, 13–18.
- [7] Wang, G., Xia, X-G., and Chen, V. C. (1999) Dual-speed SAR imaging of moving targets. Technical report UDEL#98-8-1, Dept. of Electrical and Computer Engineering, University of Delaware, 1998; also in *Proceedings of the 1999 IEEE Radar Conference*, 1999, 227–232.
- [8] Barbarossa, S., and Farina, A. (1992) Detection and imaging of moving targets with synthetic aperture radar. Part 2: Joint time-frequency analysis and Wigner-Ville distribution. *IEE Proceedings*, Pt. F, **139** (Feb. 1992), 89–97.
- [9] Barbarossa, S., and Farina, A. (1994) Space-time-frequency processing of synthetic aperture radar signals. *IEEE Transactions on Aerospace and Electronic Systems*, **30** (Apr. 1994), 341–358.
- [10] Berizzi, F., and Diani, M. (1977) Target angular motion effects on ISAR imaging. *IEE Proceedings—Radar, Sonar Navigation* **144**, 2 (1977), 87–95.

- [11] Carrara, W. G., Goodman, R. S., and Majewski, R. M. (1995)
Spotlight Synthetic Aperture Radar—Signal Processing Algorithms, Boston: Artech House, 1995.
- [12] Moreira, A., Scheiber, R., and Mittermayer, J. (1996)
Azimuth and range scaling for SAR and scan SAR processing.
In *Proceedings of IGARSS*, 1996, 1214–1216.
- [13] Chen, V. C. (1998)
Time-frequency analysis of SAR image with ground moving targets.
In *Proceedings of SPIE'98, Vol. 3391*, Orlando, FL, Apr. 1998, 295–302.
- [14] Xu, W., Chang, E. C., Kwok, L. K., Lim, H., and Heng, W. C. A. (1994)
Phase-unwrapping of SAR interferogram with multi-frequency or multi-baseline.
In *Proceedings of IGASS'94*, 1994, 730–732.
- [15] Schnitt, K., and Wiesbeck, W. (1997)
An interferometric SAR processor avoiding phase ambiguities.
In *Proceedings of IGASS'97*, 1997, 1713–1715.
- [16] Shnitkin, H. (1994)
Joint stars phase array radar antenna.
IEEE AES Magazine, (Oct. 1994), 34–41.
- [17] Wood, J., and Barry, D. (1994)
Linear signal synthesis using the Radon-Wigner transform.
IEEE Transactions on Signal Processing, **42**, 8 (1994), 2105–2111.
- [18] Cohen, L. (1995)
Time-Frequency Analysis.
Englewood Cliffs, NJ: Prentice-Hall, 1995.
- [19] Qian, S., and Chen, D. (1996)
Joint Time-Frequency Analysis: Methods and Applications.
Englewood Cliffs, NJ: Prentice-Hall, 1996.
- [20] Xia, X-G. (1999)
On estimation of multiple frequencies in undersampled complex valued waveforms.
IEEE Transactions on Signal Processing, **47** (Dec. 1999), 3417–3419.
- [21] Zhou, G. C., and Xia, X-G. (1997)
Multiple frequency detection in undersampled complex-valued waveforms with close multiple frequencies.
Electronics Letters, **33**, 15 (July 1997), 1294–1295.
- [22] Xia, X-G. (2000)
An efficient frequency determination algorithm from multiple undersampled waveforms.
IEEE Signal Processing Letters, (Feb. 2000).
- [23] McClellan, J. H., and Rader, C. M. (1979)
Number Theory in Digital Signal Processing.
Englewood Cliffs, NJ: Prentice-Hall, 1979.
- [24] Munson, D. C., Jr., O'Brien, J. D., and Jenkins, W. K. (1983)
A tomographic formulation of spotlight-mode synthetic aperture radar.
Proceedings of the IEEE, **71** (1983), 917–925.
- [25] Fiedler, R., and Jansen, R. (2000)
Adventures in SAR processing.
Proceedings of SPIE, Orlando, FL, Apr. 2000.
- [26] Bamler, R. (1992)
A comparison of range-Doppler and wave number domain SAR focusing algorithms.
IEEE Transactions on Geoscience and Remote Sensing **30** (July 1992), 706–713.
- [27] Brown, W. M., and Fredricks, R. J. (1991)
Range-Doppler imaging with motion through resolution cells.
IEEE Transactions on Aerospace and Electronic Systems, **27** (Mar. 1991), 194–207.
- [28] Soumekh, M. (1999)
Synthetic Aperture Radar Signal Processing with MATLAB Algorithms.
New York: Wiley, 1999.
- [29] Soumekh, M. (1997)
Moving target detection in foliage using along track monopulse synthetic aperture radar imaging.
IEEE Transactions on Image Processing, **6**, 8 (Aug. 1997), 1148–1163.

Design of Frequency Modulated Waveforms via the Zak Transform

This paper introduces a new technique for designing frequency modulated waveforms that have ambiguity functions with desirable properties, such as strong peaking at the origin and low sidelobes. The methods employed involve signal design in Zak transform space, as well as the use of stationary phase arguments in the analysis of ambiguity functions.

I. INTRODUCTION. DEFINITIONS AND SOME PROPERTIES OF AMBIGUITY FUNCTION AND ZAK TRANSFORM

DEFINITION 1 The ambiguity function of a finite energy pulse $s(t)$ is a function of $s(t)$ given by the complex function of two variables [2]:

$$A_s(\tau, \nu) = \int_{-\infty}^{+\infty} s(t)\overline{s(t-\tau)}e^{-2\pi i\nu t} dt \quad (1)$$

where $\overline{s(t)}$ denotes the complex conjugate of $s(t)$. The magnitude of the ambiguity function $|A(\tau, \nu)|^2$ is called the ambiguity surface.

The following are the main properties of the ambiguity function:

- 1) $A_s(0, 0) = \|s\|^2$.
- 2) $|A_s(\tau, \nu)| < A_s(0, 0)$, $(\tau, \nu) \neq (0, 0)$, (maximum property).

- 3) Let $g(t) = s(t-x)e^{-2\pi i y t}$, then

$$A_g(\tau, \nu) = A_s(\tau, \nu)e^{-2\pi i(x\nu + y\tau)}.$$

- 4) $A_s(\tau, \nu) = \overline{A_s(-\tau, -\nu)}$, (symmetry property).

Manuscript received November 16, 2001; revised July 30, 2002 and February 19, 2003; released for publication November 10, 2003.

IEEE Log No. T-AES/40/1/826484.

Refereeing of this contribution was handled by S. S. Chornoboy.

0018-9251/04/\$17.00 © 2004 IEEE